LETTER

doi:10.1038/nature22340

Isotopic evidence of multiple controls on atmospheric oxidants over climate transitions

Lei Geng[1,2,3], Lee T. Murray[4], Loretta J. Mickley[5], Pu Lin[6], Qiang Fu[1], Andrew J. Schauer[7] & Becky Alexander[1]

The abundance of tropospheric oxidants, such as ozone (O_3) and hydroxyl (OH) and peroxy radicals ($HO_2 + RO_2$), determines the lifetimes of reduced trace gases such as methane and the production of particulate matter important for climate and human health. The response of tropospheric oxidants to climate change is poorly constrained owing to large uncertainties in the degree to which processes that influence oxidants may change with climate[1] and owing to a lack of palaeo-records with which to constrain levels of atmospheric oxidants during past climate transitions[2]. At present, it is thought that temperature-dependent emissions of tropospheric O_3 precursors and water vapour abundance determine the climate response of oxidants, resulting in lower tropospheric O_3 in cold climates while HO_x ($= OH + HO_2 + RO_2$) remains relatively buffered[3]. Here we report observations of oxygen-17 excess of nitrate (a proxy for the relative abundance of atmospheric O_3 and HO_x) from a Greenland ice core over the most recent glacial–interglacial cycle and for two Dansgaard–Oeschger events. We find that tropospheric oxidants are sensitive to climate change with an increase in the O_3/HO_x ratio in cold climates, the opposite of current expectations. We hypothesize that the observed increase in O_3/HO_x in cold climates is driven by enhanced stratosphere-to-troposphere transport of O_3, and that reactive halogen chemistry is also enhanced in cold climates. Reactive halogens influence the oxidative capacity of the troposphere directly as oxidants themselves and indirectly[4] via their influence on O_3 and HO_x. The strength of stratosphere-to-troposphere transport is largely controlled by the Brewer–Dobson circulation[5], which may be enhanced in colder climates owing to a stronger meridional gradient of sea surface temperatures[6], with implications for the response of tropospheric oxidants[7] and stratospheric thermal and mass balance[8]. These two processes may represent important, yet relatively unexplored, climate feedback mechanisms during major climate transitions.

The oxygen-17 excess ($\Delta^{17}O = \delta^{17}O - 0.52 \times \delta^{18}O$) of ice-core nitrate is suggested to be one of the most promising proxies for reconstructing atmospheric oxidation capacity[2]. Greenland ice-core nitrate originates from deposition of atmospheric nitrate that formed in the Northern Hemisphere mid-latitude NO_x-source regions. Globally, atmospheric nitrate is formed mainly[9] via oxidation of NO_x by HO_x or O_3. Oxidation of NO_x by reactive bromine (BrO) may also be important in the marine boundary layer[10] and during short-lived episodes such as polar ozone depletion events in Arctic spring[11]. O_3- and BrO-dominated reactions lead to high $\Delta^{17}O$ values in atmospheric nitrate, while HO_x-dominated reactions lead to low $\Delta^{17}O$ (section 1 of the Supplementary Information). The value of $\Delta^{17}O$ in ice-core nitrate ($\Delta^{17}O(NO_3^-)$) can thus provide information on these oxidants in past atmospheres, and is particularly sensitive to the ratio of $O_3/(HO_2 + RO_2)$ (where R represents a hydrocarbon chain; section 1 of the Supplementary Information).

The glacial–interglacial ice-core record of $\Delta^{17}O(NO_3^-)$ (Fig. 1a) displays a negative correlation with a proxy for local Greenland temperature ($\delta^{18}O(H_2O)$) ($r = -0.76$, $P < 0.01$, Fig. 2a). Throughout the record, two samples fall within two Heinrich events (H1 at about 16,800 years ago (16.8 kyr ago) and H2 at 23 kyr ago) within or near the last glacial maximum (LGM, 19–23 kyr ago)[12]. These two samples are in glacial climate conditions analogous to that in the LGM. We use the mean $\Delta^{17}O(NO_3^-)$ of these two samples to represent glacial $\Delta^{17}O(NO_3^-)$, which is 35.5‰ ± 0.7‰. Comparing the glacial $\Delta^{17}O(NO_3^-)$ to the mean of the four Holocene samples ($\Delta^{17}O(NO_3^-) = 29.4‰ \pm 0.7‰$) yields a glacial–Holocene difference of around 6.2‰. The high-resolution record of $\Delta^{17}O(NO_3^-)$ over two abrupt climate change events (Dansgaard–Oeschger events DO-12 and DO-13; see Fig. 1b) shows that $\Delta^{17}O(NO_3^-)$ responds rapidly to abrupt warming and cooling. In particular, immediately following the abrupt warming (an increase of about 10 °C over about 100 years in Greenland[12]) from GS-13 (Greenland Stadial 13, the cold phase of DO-13) to GS-12 (the warm phase of DO-12), $\Delta^{17}O(NO_3^-)$ decreased by 2.3‰ ± 0.2‰, a temperature-dependent response in the same direction as that on the glacial–interglacial timescale (Figs 1 and 2).

Closer evaluation of the relationship between $\Delta^{17}O(NO_3^-)$ and temperature over Dansgaard–Oeschger events reveals two regimes (Fig. 2b). During the relatively warm period (43.9–45.4 kyr ago, that is, GS-12 and the onset of its cooling), $\Delta^{17}O(NO_3^-)$ decreases moderately with decreasing temperature ($r = 0.40$, $P < 0.01$), opposite to the trend observed on the glacial–interglacial timescale. In contrast, during the relatively cold periods of these two Dansgaard–Oeschger events, $\Delta^{17}O(NO_3^-)$ increases strongly with decreasing temperature ($r = -0.82$, $P < 0.01$), similar to the direction of the trend on the glacial–interglacial timescale. We note that this two-regime relationship observed in the Dansgaard–Oeschger events may also exist over the glacial–interglacial cycle, but is impossible to statistically extract with the limited sample size we have over this time period.

Results from the ICECAP (ICE age Chemistry And Proxies) model[3] (Methods) show decreases in tropospheric O_3 and $(HO_2 + RO_2)$ abundances in cold climates compared to warm climates throughout the northern mid- to high latitudes (Fig. 3a and b). The modelled fraction of NO oxidized by O_3 (versus $HO_2 + RO_2$ oxidation) in NO_x cycling (represented by the A value; see section 1 of the Supplementary Information and Supplementary Information Table 1), which explicitly determines $\Delta^{17}O(NO_2)$ and thus two-thirds of the value of $\Delta^{17}O(NO_3^-)$ (see section 1.1 of the Supplementary Information), also decreases in colder climates (Fig. 3c). This suggests that changes in $O_3/(HO_2 + RO_2)$ ratio (Fig. 3d) driven by temperature-dependent emissions of tropospheric O_3 precursors tend to lower $\Delta^{17}O(NO_3^-)$ in the glacial period compared to the Holocene, opposite to the observations.

Oxidation of NO_2 to HNO_3 (for example, OH versus O_3 oxidation) determines one-third of the value of $\Delta^{17}O(NO_3^-)$ and may also vary with climate (section 2 of the Supplementary Information). Using ICECAP, we find that climate-driven changes in the oxidation

[1]Department of Atmospheric Sciences, University of Washington, Seattle, Washington 98195, USA. [2]Institut des Géosciences de l'Environnement, Université Grenoble Alpes, Grenoble 38508, France. [3]School of Earth and Space Sciences, University of Science and Technology of China, Hefei 230026, Anhui, China. [4]Department of Earth and Environmental Sciences, University of Rochester, Rochester, New York, USA. [5]School of Engineering and Applied Sciences, Harvard University, Cambridge, Massachusetts, USA. [6]Program in Atmospheric and Oceanic Sciences, Princeton University, Princeton, New Jersey, USA. [7]Department of Earth and Space Sciences, University of Washington, Seattle, Washington 98195, USA.

© 2017 Macmillan Publishers Limited, part of Springer Nature. All rights reserved.

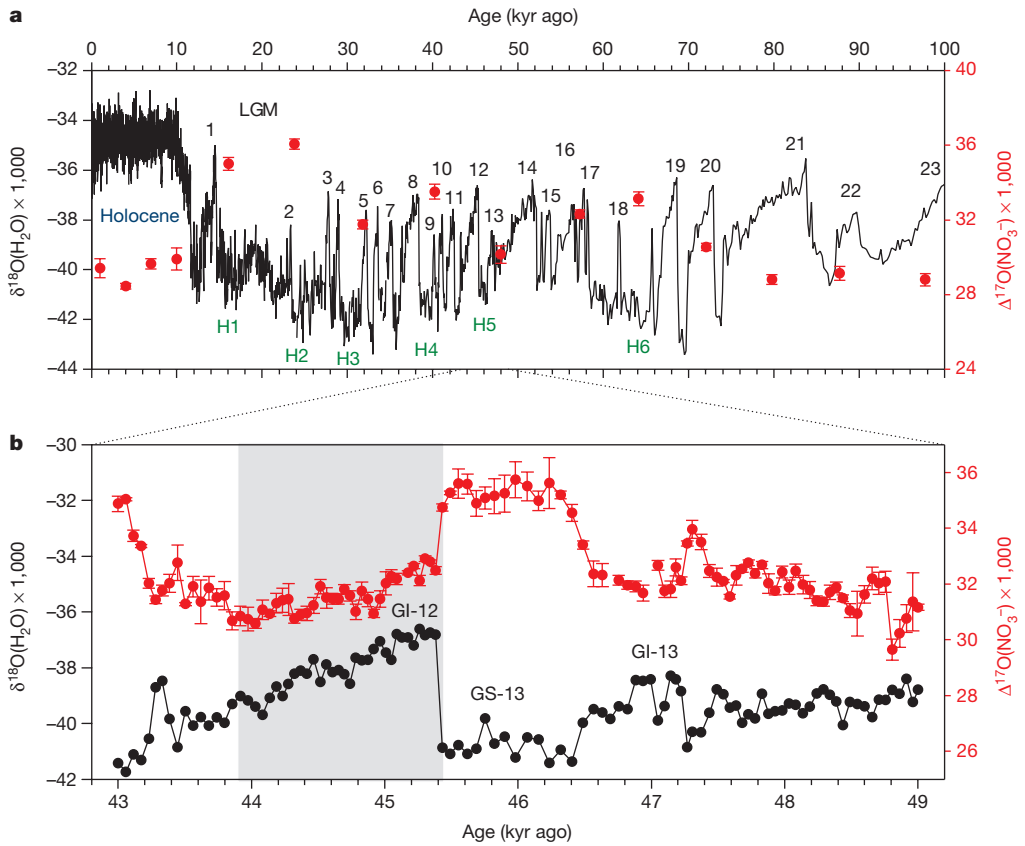

Figure 1 | GISP2 ice-core record of $\Delta^{17}O(NO_3^-)$. $\Delta^{17}O(NO_3^-)$ from the last 100 kyr (**a**), and DO-12 and DO-13 (**b**). $\delta^{18}O(H_2O)$ is a local Greenland temperature proxy, varying similarly to Northern Hemisphere temperatures on these timescales[12]. High-resolution $\delta^{18}O(H_2O)$ values in **a** are from ref. 29, and in **b** are from this study. Numbers in **a** represent Dansgaard–Oeschger events, and H1–H6 represent Heinrich events[12]. GI and GS in **b** represent Greenland interstadial and stadial stages. The shaded area in **b** indicates the warm period of DO-12. The symbols and error bars represent the mean and one standard deviation of $\Delta^{17}O(NO_3^-)$ from triplicate ($n = 3$) measurements.

of NO_2 to HNO_3 tend to lower $\Delta^{17}O(NO_3^-)$ in colder climates, except for changes in $BrONO_2$ hydrolysis (see section 1.2 of the Supplementary Information and Supplementary Information Table 1). In ICECAP, the relative importance of nitrate formation via $BrONO_2$ hydrolysis in cold climates increases owing to modelled higher glacial BrO concentrations relative to the Holocene (section 1.2 of the Supplementary Information). Increased BrO in the model is primarily driven by decreases in glacial HO_2, which is the largest sink of BrO_x (= Br + BrO). Increases in reactive Br production from increased HOBr photolysis caused by reductions in other HOBr loss pathways (for example, wet deposition) and increased polar photolysis rates also play a part[3]. Modelled changes in $BrONO_2$ hydrolysis alone tend to increase glacial $\Delta^{17}O(NO_3^-)$ by 1.0–2.5‰. However, given the modelled lowered glacial A value, $\Delta^{17}O(NO_3^-)$ in the LGM decreases by 2.5–3.3‰ compared to the Holocene (see Supplementary Information Table 1). With this lower A value, in order for increases in $BrONO_2$ hydrolysis to explain the magnitude of the observed glacial–interglacial change in $\Delta^{17}O(NO_3^-)$, such hydrolysis must account for 70–82% of total nitrate production in the northern mid- to high latitudes in the glacial period. $BrONO_2$ hydrolysis contributes only 20% ± 10% to total nitrate production in high-halogen environments (that is, the tropical marine boundary layer) in the present-day atmosphere[10]. In the polar regions after polar sunrise when O_3 depletion events occur[13], $BrONO_2$ hydrolysis may dominate local nitrate production[11]. However, these short-lived episodes are constrained to polar springtime and do not represent the major nitrate production pathways over the larger spatial and temporal scales recorded in Greenland ice cores. The relative importance of $BrONO_2$ hydrolysis for nitrate production may be underestimated by ICECAP owing to missing sources of halogens, such as the sea-ice source (section 1.2 of the Supplementary Information). No model studies have yet investigated the climate sensitivity of reactive halogen chemistry.

Modelling studies suggest an increase in stratosphere-to-troposphere transport (STT) of O_3 in the glacial climate driven by an enhanced Brewer–Dobson circulation (BDC)[6,14], which would tend to increase $\Delta^{17}O(NO_3^-)$ by increasing the concentration of tropospheric O_3; this is

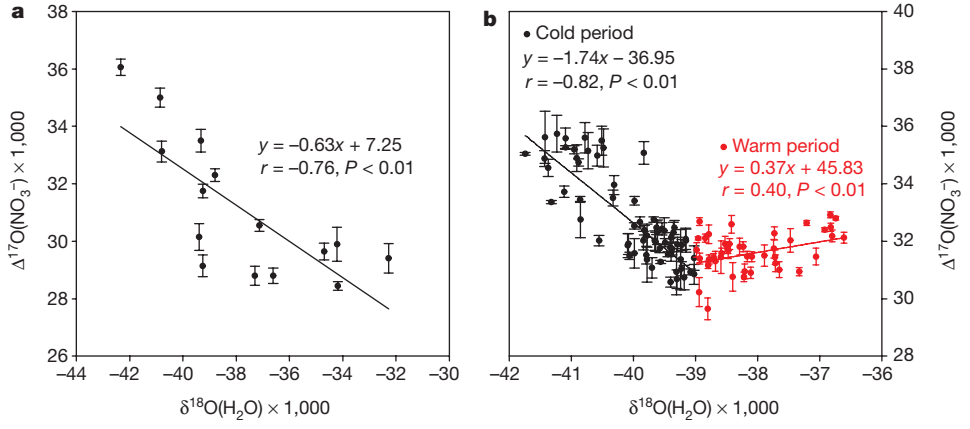

Figure 2 | Relationship between measured $\delta^{18}O(H_2O)$ and $\Delta^{17}O(NO_3^-)$. **a**, $\Delta^{17}O(NO_3^-)$ during the glacial–interglacial period. **b**, DO-12 and DO-13 in the period 43–49 kyr ago. Red data in **b** represent observations during the relatively warm period (GI-12 and its onset of cooling during the period 43.9–45.4 kyr ago) of DO-12 and DO-13, while black data represent the observations during the relatively cold period. The symbols and error bars represent the mean and one standard deviation of $\Delta^{17}O(NO_3^-)$ from triplicate ($n = 3$) measurements. The linear regression equations, with the r and the P values, are shown for each fit.

© 2017 Macmillan Publishers Limited, part of Springer Nature. All rights reserved.

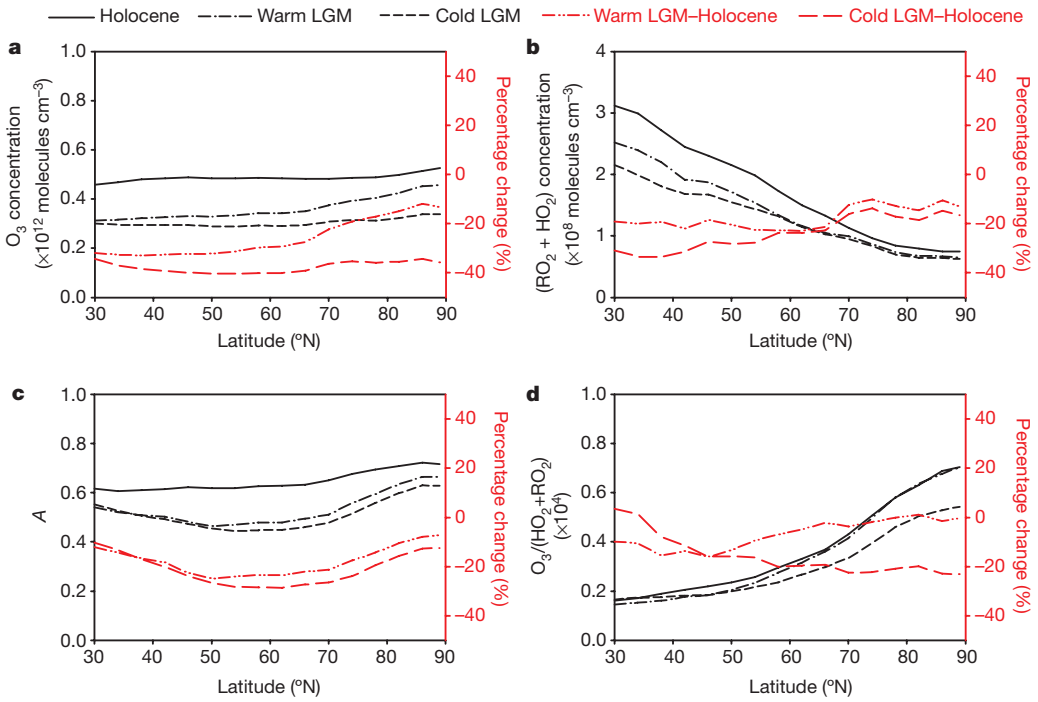

Figure 3 | ICECAP model results of zonal mean tropospheric oxidants in the Holocene and glacial climates. a–d, Zonal-mean O_3 concentrations (**a**), $HO_2 + RO_2$ concentrations (**b**), the *A* value (**c**) and the $O_3/(HO_2 + RO_2)$ ratio (**d**) in the Northern mid- to high latitudes are shown. Also shown is the relative difference between the glacial and Holocene (percentage change). The glacial climate is represented by two different global temperature reconstruction scenarios, the warm LGM from CLIMAP[30] and the cold LGM from ref. 31. These model results consider the impact of changes in precursor emissions and chemistry only.

qualitatively consistent with the observations. The BDC is characterized by tropospheric air entering the stratosphere in the tropics and moving poleward before descending in the extratropics[5]. The BDC is comprised of a shallow branch that passes through the lowermost stratosphere and re-enters the troposphere in the subtropics and mid-latitudes, and a deep branch that rises to the upper stratosphere before descending in the mid- and high latitudes[15]. Enhanced STT mass exchange driven by a stronger BDC can therefore lead to enhanced tropospheric ozone in the mid- to high latitudes[7]. Modelled increases in glacial STT are driven by increased sea surface temperature (SST) gradients between the tropics and mid- to high latitudes during glacial periods relative to the present, which acts to increase vertical wave propagation in the mid-latitudes despite lower greenhouse gas levels[6]. This is consistent with ref. 16 who found that the BDC intensifies in response to a stronger SST gradient from the tropics through the mid-latitudes in model simulations of the recent past, with or without an increasing atmospheric greenhouse gas burden. In addition, although the total stratospheric O_3 column abundance is predicted to increase only by a few per cent in the LGM owing to a warmer stratospheric temperature (radiative influence) and the altered atmospheric composition and dynamics compared to the Holocene[6], the lowermost stratospheric ozone in the mid- to high latitudes may have been further enhanced by an acceleration of the BDC. As a result, STT may have been stronger in the glacial period compared to the Holocene, leading to regional increases in tropospheric O_3, particularly in the Northern Hemisphere as predicted by global climate model simulations[3,6].

A stronger STT flux of O_3 tends to increase $\Delta^{17}O(NO_3^-)$ through increasing the relative importance of O_3 in the oxidation of NO and NO_2. Increases in O_3 abundance will also tend to increase reactive halogen abundance[17] and potentially the extent of $BrONO_2$ hydrolysis (and hence the formation of nitrate through this pathway), in addition to increasing the amount of night-time relative to daytime nitrate production (section 2 of the Supplementary Information). Taking all of these reactions into account, we estimate that in the northern mid-to high-latitude troposphere, the tropospheric abundance of stratospheric-sourced O_3 in the glacial climate would need to increase by 118–252% relative to the Holocene, in order to explain the observed 6.2‰ increase in $\Delta^{17}O(NO_3^-)$. Because reactive halogen chemistry in the LGM may be underestimated by ICECAP (section 3 of the Supplementary Information), these values reflect the high-end possible change in STT of O_3 in the LGM, and are much higher than the model-simulated 11% increase in the downward transport of O_3 through the 200-mbar level in the extratropics from the Holocene to LGM[6]. We note that increases in stratospheric-sourced O_3 by STT flux may be a result of a variety of processes, caused not only by an enhanced BDC but also increased stratospheric O_3 abundance due to lower methane (CH_4) and N_2O abundances in the glacial climate, and/or increases in synoptic-scale processes such as tropopause folding events[18,19]. More research is required to examine the causes, and to assess the magnitude, of potential changes in STT in the glacial climate.

The response of $\Delta^{17}O(NO_3^-)$ to temperature during the abrupt warming and cooling transitions of the Dansgaard–Oeschger events (Figs 1b and 2b) is also consistent with the effect of variations in meridional SST gradient on the strength of the BDC and STT flux of O_3. The temperature changes over the course of a Dansgaard–Oeschger event are associated with variations in the strength of the Atlantic Meridional Overturning Circulation (AMOC)[20,21]. The AMOC impacts the meridional gradient of SST in the Northern Hemisphere[22], with stronger AMOC resulting in weaker SST gradient, and vice versa. The latter in turn leads to changes in the BDC and thus STT[16]. The rapid resumption of the AMOC during the abrupt warming of a Dansgaard–Oeschger event[20,21] suggests a rapid slowdown of the BDC and STT, leading to decreases in tropospheric O_3 and thus in $\Delta^{17}O(NO_3^-)$ in the northern mid- to high latitudes. In contrast, during the abrupt cooling of a Dansgaard–Oeschger event, the AMOC rapidly declines[20,21], which may lead to rapid increases in the BDC and STT, resulting in increases in tropospheric O_3 and thus in $\Delta^{17}O(NO_3^-)$. Changes in the abundance of reactive halogens via, for example, changes in the sea-ice source may also affect $\Delta^{17}O(NO_3^-)$ during abrupt climate changes, similar in direction to changes on the glacial–interglacial timescale.

During the smaller, more gradual climate changes in DO-12 and DO-13, for example, in the relatively warm period after the abrupt warming approximately 45.4 kyr ago, the observations indicate a positive relationship between $\Delta^{17}O(NO_3^-)$ and temperature. During this relatively warm period, variability in the regional abundance of tropospheric O_3 was probably controlled by changes in temperature-dependent emissions of O_3-precursor gases. Surface temperatures slowly decline during the warm period, decreasing O_3 precursor emissions and tropospheric O_3 production. These decreases tend to lower

© 2017 Macmillan Publishers Limited, part of Springer Nature. All rights reserved.

O_3/HO_x and thus $\Delta^{17}O(NO_3^-)$ as long as O_3 decreases more than HO_x, consistent with our ICECAP model simulations (Fig. 3d).

Our hypothesized response of the BDC to climate runs counter to the prediction of an acceleration of the BDC in response to increasing greenhouse gas concentrations. However, it is the shallow instead of the deep branch of the BDC that accelerates with increasing greenhouse gases from the recent past through the near future to 2100[15] owing to increasing wave propagation from the subtropical troposphere[23], a conclusion with which climate models robustly agree. Furthermore, if future Arctic amplification[24] offsets the effect of increasing greenhouse gases on the meridional SST gradient[16] in the Northern Hemisphere, model predictions of future intensification of the BDC in response to increased greenhouse gases[25] might be offset.

Increases in reactive halogen chemistry and the BDC might have important implications for the oxidation capacity of the atmosphere in cold climates. Increases in the BDC in cold climates would influence global tropospheric OH abundance by altering the spatial distribution of stratospheric O_3 and thus ultraviolet-photolysis rates in the troposphere[3]. Enhanced transport of stratospheric O_3 from the Equator to the poles caused by a stronger BDC lowers the overhead O_3-column abundance in the tropics and elevates it in the polar regions[7]. All else being equal, this will increase OH production in the tropics and decrease OH production in the mid- to high latitudes[3]. Changes in tropical OH are particularly important for understanding the global CH_4 budget because it is the OH abundance in the tropics that is most relevant for the CH_4 lifetime[26]. A stronger BDC in the last glacial period, which would reduce the tropical stratospheric ozone column, should alone lead to enhanced tropical OH production and a shorter CH_4 lifetime. Enhanced reactive halogen chemistry in the LGM may also tend to influence the CH_4 lifetime directly via the chlorine radical sink[27] and indirectly via its influence on OH[4]. Climate-driven changes in the BDC and reactive halogen chemistry and their impacts on the oxidizing capacity of the atmosphere may need to be considered to reconcile global CH_4 variations during glacial–interglacial and abrupt climate changes[28].

Online Content Methods, along with any additional Extended Data display items and Source Data, are available in the online version of the paper; references unique to these sections appear only in the online paper.

Received 9 March 2016; accepted 30 March 2017.
Published online 17 May 2017.

1. Naik, V. *et al.* Preindustrial to present-day changes in tropospheric hydroxyl radical and methane lifetime from the Atmospheric Chemistry and Climate Model Intercomparison Project (ACCMIP). *Atmos. Chem. Phys.* **13,** 5277–5298 (2013).
2. Alexander, B. & Mickley, L. Paleo-perspectives on potential future changes in the oxidative capacity of the atmosphere due to climate change and anthropogenic emissions. *Curr. Pollution Rep.* **1,** 57–69 (2015).
3. Murray, L. T. *et al.* Factors controlling variability in the oxidative capacity of the troposphere since the Last Glacial Maximum. *Atmos. Chem. Phys.* **14,** 3589–3622 (2014).
4. Schmidt, J. A. *et al.* Modeling the observed tropospheric BrO background: importance of multiphase chemistry and implications for ozone, OH, and mercury. *J. Geophys. Res.* **121,** 11819–11835 (2016).
5. Holton, J. R. *et al.* Stratosphere-troposphere exchange. *Rev. Geophys.* **33,** 403–439 (1995).
6. Rind, D., Lerner, J., McLinden, C. & Perlwitz, J. Stratospheric ozone during the Last Glacial Maximum. *Geophys. Res. Lett.* **36,** L09712 (2009).
7. Hegglin, M. I. & Shepherd, T. G. Large climate-induced changes in ultraviolet index and stratosphere-to-troposphere ozone flux. *Nat. Geosci.* **2,** 687–691 (2009).
8. Butchart, N. The Brewer-Dobson circulation. *Rev. Geophys.* **52,** 157–184 (2014).
9. Alexander, B. *et al.* Quantifying atmospheric nitrate formation pathways based on a global model of the oxygen isotopic composition ($\Delta^{17}O$) of atmospheric nitrate. *Atmos. Chem. Phys.* **9,** 5043–5056 (2009).
10. Savarino, J. *et al.* Isotopic composition of atmospheric nitrate in a tropical marine boundary layer. *Proc. Natl Acad. Sci. USA* **110,** 17668–17673 (2013).
11. Morin, S., Savarino, J., Bekki, S., Gong, S. & Bottenheim, J. W. Signature of Arctic surface ozone depletion events in the isotope anomaly ($\Delta^{17}O$) of atmospheric nitrate. *Atmos. Chem. Phys.* **7,** 1451–1469 (2007).
12. Alley, R. B. Wally was right: predictive ability of the North Atlantic "Conveyor Belt" hypothesis for abrupt climate change. *Annu. Rev. Earth Planet. Sci.* **35,** 241–272 (2007).
13. Barrie, L. A., Bottenheim, J. W., Schnell, R. C., Crutzen, P. J. & Rasmussen, R. A. Ozone destruction and photochemical reactions at polar sunrise in the lower Arctic atmosphere. *Nature* **334,** 138–141 (1988).
14. Rind, D., Chandler, M., Lonergan, P. & Lerner, J. Climate change and the middle atmosphere. 5. Paleostratosphere in cold and warm climates. *J. Geophys. Res.* **106,** 20195–20212 (2001).
15. Lin, P. & Fu, Q. Changes in various branches of the Brewer–Dobson circulation from an ensemble of chemistry climate models. *J. Geophys. Res.* **118,** 73–84 (2013).
16. Olsen, M. A., Schoeberl, M. R. & Nielsen, J. E. Response of stratospheric circulation and stratosphere-troposphere exchange to changing sea surface temperatures. *J. Geophys. Res.* **112,** (2007).
17. Sherwen, T., Evans, M. J., Carpenter, L. J., Schmidt, J. A. & Mickley, L. J. Halogen chemistry reduces tropospheric O_3 radiative forcing. *Atmos. Chem. Phys.* **17,** 1557–1569 (2017).
18. Sprenger, M., Wernli, H. & Bourqui, M. Stratosphere–troposphere exchange and its relation to potential vorticity streamers and cutoffs near the extratropical tropopause. *J. Atmos. Sci.* **64,** 1587–1602 (2007).
19. Xie, B., Zhang, H., Wang, Z., Zhao, S. & Fu, Q. A modeling study of effective radiative forcing and climate response due to tropospheric ozone. *Adv. Atmos. Sci.* **33,** 819–828 (2016).
20. Knutti, R., Fluckiger, J., Stocker, T. F. & Timmermann, A. Strong hemispheric coupling of glacial climate through freshwater discharge and ocean circulation. *Nature* **430,** 851–856 (2004).
21. McManus, J. F., Francois, R., Gherardi, J. M., Keigwin, L. D. & Brown-Leger, S. Collapse and rapid resumption of Atlantic meridional circulation linked to deglacial climate changes. *Nature* **428,** 834–837 (2004).
22. Persechino, A. *et al.* Decadal-timescale changes of the Atlantic overturning circulation and climate in a coupled climate model with a hybrid-coordinate ocean component. *Clim. Dyn.* **39,** 1021–1042 (2012).
23. Shepherd, T. G. & McLandress, C. A robust mechanism for strengthening of the Brewer–Dobson circulation in response to climate change: critical-layer control of subtropical wave breaking. *J. Atmos. Sci.* **68,** 784–797 (2011).
24. Miller, G. H. *et al.* Arctic amplification: can the past constrain the future? *Quat. Sci. Rev.* **29,** 1779–1790 (2010).
25. Butchart, N. *et al.* Simulations of anthropogenic change in the strength of the Brewer-Dobson circulation. *Clim. Dyn.* **27,** 727–741 (2006).
26. Holmes, C. D., Prather, M. J., Sovde, O. A. & Myhre, G. Future methane, hydroxyl, and their uncertainties: key climate and emission parameters for future predictions. *Atmos. Chem. Phys.* **13,** 285–302 (2013).
27. Allan, W., Struthers, H. & Lowe, D. C. Methane carbon isotope effects caused by atomic chlorine in the marine boundary layer: global model results compared with Southern Hemisphere measurements. *J. Geophys. Res.* **112,** D04306 (2007).
28. Brook, E. J., Sowers, T. & Orchardo, J. Rapid variations in atmospheric methane concentration during the past 110,000 years. *Science* **273,** 1087–1091 (1996).
29. Grootes, P. M. & Stuiver, M. Oxygen 18/16 variability in Greenland snow and ice with 10^{-3}- to 10^5-year time resolution. *J. Geophys. Res.* **102,** 26455–26470 (1997).
30. CLIMAP. The surface of the ice-age Earth. *Science* **191,** 1131–1137 (1976).
31. Webb, R. S., Rind, D. H., Lehman, S. J., Healy, R. J. & Sigman, D. Influence of ocean heat transport on the climate of the Last Glacial Maximum. *Nature* **385,** 695–699 (1997).

Supplementary Information is available in the online version of the paper.

Acknowledgements We acknowledge financial support from NSF awards AGS 1103163, PLR 1106317 and PLR 1244817 (to B.A.) and AGS 1102880 (to L.J.M. and L.T.M.). L.T.M. was also supported by the NASA Postdoctoral Program Fellowship administered by Oak Ridge Associated Universities (NNH06CC03B). Q.F. is supported by NASA Grant NNX13AN49G. P.L. is supported by NA14OAR4320106 from the National Oceanic and Atmospheric Administration, the US Department of Commerce. The statements, findings, conclusions, and recommendations are those of the author(s) and do not necessarily reflect the views of the National Oceanic and Atmospheric Administration, or the US Department of Commerce. We thank the National Ice Core Laboratory for providing the GISP2 ice-core samples, and the GISP2 team for ice-core drilling. We also thank our laboratory technician B. Vanden Heuvel for measurements of $\delta^{18}O(H_2O)$.

Author Contributions B.A. conceived the study; L.G. performed the measurements, analysed the experimental and model data, proposed the hypotheses and wrote the manuscript with B.A.; L.T.M. constructed the ICECAP model under the supervision of L.J.M., and provided the model results; L.T.M., P.L. and Q.F. contributed to the hypotheses; A.J.S. assisted with the laboratory work. All authors contributed to the data interpretation and writing.

Author Information Reprints and permissions information is available at www.nature.com/reprints. The authors declare no competing financial interests. Readers are welcome to comment on the online version of the paper. Publisher's note: Springer Nature remains neutral with regard to jurisdictional claims in published maps and institutional affiliations. Correspondence and requests for materials should be addressed to B.A. (beckya@uw.edu).

Reviewer Information *Nature* thanks T. Roeckmann and the other anonymous reviewer(s) for their contribution to the peer review of this work.

© 2017 Macmillan Publishers Limited, part of Springer Nature. All rights reserved.

METHODS

Sample collection and laboratory analysis. The samples are from the Greenland Ice Sheet Project 2 (GISP2, Summit, Greenland, 72.6° N, 38.5° W, 3,200 m elevation, 0.24 m of ice per year at present[32]) ice core. We collected 15 discrete samples (around 2 kg of ice each) at depths between 264 m and 2,735 m covering the last glacial–interglacial cycle (approximately 1–100 kyr ago). Each sample spans a depth of about 50 cm depth, representing 2–200 years of snow accumulation. Another 112 continuous samples throughout the depth interval of 2,310 m to 2,413 m were collected, covering the DO-12 and DO-13 cycles occurring in the period 43–49 kyr ago[29]. The length of each sample is 0.8–1.0 m, representing about 50 years of snow accumulation. All samples were decontaminated by removing the surface layer (about 0.5 cm) with a band saw in a cold room (−8 °C) followed by rinsing with 18 MΩ cm^{-1} water. The samples were then placed in covered, pre-cleaned beakers and melted at room temperature in a clean, laminar-flow hood. After melting, nitrate in the discrete samples was concentrated using an ion chromatograph[33] and nitrate in the continuous samples was concentrated using the resin method[34].

In IsoLab (http://isolab.ess.washington.edu/isolab/) at the University of Washington, the concentrated samples were then measured for $\Delta^{17}O(NO_3^-)$ in triplicate using the bacterial denitrifier method with a gold tube[35] on a Delta Plus Advantage isotope ratio mass spectrometer. Briefly, denitrifying bacteria convert NO_3^- to N_2O, which is decomposed to O_2 and N_2 in a heated gold tube at 800 °C. The thermal products of O_2 and N_2 are separated by a gas chromatograph, followed by the measurement of the mass/charge (m/z) of 28 and 29 from N_2, and m/z of 32, 33 and 34 from O_2. The mass ratios of $^{33}O_2/^{32}O_2$ and $^{34}O_2/^{32}O_2$ are converted to atomic ratios of $^{17}O/^{16}O$ and $^{18}O/^{16}O$, respectively. The atomic ratios are then converted to delta notation, $\delta^{17}O$ and $\delta^{18}O$, with respect to the Vienna Standard Mean Ocean Water (VSMOW), where $\delta = (^xO/^{16}O_{sample})/(^xO/^{16}O_{VSMOW}) - 1$ with $x = 17$ or 18. The $\delta^{17}O$ and $\delta^{18}O$ values are normalized to the VSMOW scale using two international reference materials USGS34 ($\delta^{17}O = -14.5‰$, $\delta^{18}O = -27.9‰$) and USGS35 ($\delta^{17}O = 51.3‰$, $\delta^{18}O = 57.5‰$)[35], with a 1:1 mixture of USGS34 and USGS35 used as a quality control standard. The $\Delta^{17}O$ values are then calculated using the linear approximation $\Delta^{17}O \approx \delta^{17}O - 0.52 \times \delta^{18}O$. The analytical uncertainty of $\Delta^{17}O(NO_3^-)$ was ±0.1‰, based on repeated measurements of the quality control standard.

$\delta^{18}O(H_2O)$ of the 15 glacial–interglacial samples and the 112 samples from the DO-12 and DO-13 events are also measured in IsoLab using a Cavity Ring-down Spectrometer[36] (Picarro L-2120i). $\delta^{18}O(H_2O)$ is expressed relative to VSMOW using in-house reference waters that were previously measured against VSMOW and SLAP (Standard Light Antarctic Precipitation) international reference waters. The measured $\delta^{18}O(H_2O)$ of each sample is almost identical to the averaged $\delta^{18}O(H_2O)$ over the same depth interval calculated from the high-resolution data reported by ref. 29.

The ICECAP model. The ICECAP model is a climate–biosphere–chemistry modelling framework for simulating the chemical composition of the atmosphere at and since the LGM[3]. In ICECAP, the climate is simulated by the GISS ModelE, which is forced by reconstructed greenhouse gas levels, sea surface temperatures, orbital parameters, topography, and sea-ice coverage. The ModelE meteorological fields are applied to two global vegetation models: BIOME4-TG[37] to determine land-cover characteristics, and LPJ-LMfire[38] to calculate dry matter consumed by fires. Model-E meteorology and the land cover products are then used to drive the GEOS-Chem Chemical Transport Model of tropospheric composition[3]. With this framework, we can test the sensitivity of tropospheric oxidants to diverse controlling factors across a range of uncertainty.

ICECAP also simulates stratospheric O_3 using the Linoz linearized chemical scheme and an array of about 20 species in the stratosphere in order to account for the chemical fluxes, including O_3, across the tropopause. ICECAP predicts increased STT during the LGM relative to the Holocene in some regions of the Northern Hemisphere, qualitatively consistent with the observations. However, we have little confidence that the model captures the magnitudes of changes in STT across climate transitions. The simulations of the ICECAP model used are known to have a high bias in the polar stratosphere-to-troposphere air-mass flux, which leads to a large overestimation of the stratospheric ozone flux despite reasonable stratospheric ozone concentrations[3]. This is probably due to the relatively coarse vertical resolution of this version of ModelE, which provides the meteorology for use in GEOS-Chem. The coarse vertical resolution may also cause ModelE to not fully resolve features such as tropopause folding events that can contribute substantially to local stratosphere–troposphere exchange. The low vertical resolution in ModelE may also lead to bias in the wave propagation from the troposphere into the stratosphere. Furthermore, climate models lacking resolved mesosphere dynamics such as Model-E require parameterizations of the gravity wave drag force that drives the BDC. Previous studies have shown that the simulated stratospheric climate is sensitive to the choice of gravity wave drag parameterization in the model (ref. 39 and references therein). Such parameterization is employed to represent the small-scale gravity waves that transport momentum from the troposphere and surface to the middle atmosphere. These waves are small in scale and intermittent in occurrence, and have few observational constraints. The change of these gravity waves under different climate and surface orographies such as the LGM is even less constrained. Therefore, we don't use the ICECAP model to explicitly interpret the STT changes in this work.

For these reasons, we use ICECAP only to investigate the sensitivity of tropospheric O_3 and HO_x abundances to precursor emissions and chemistry and not to STT. We calculate tropospheric O_3 production in each climate regime according to their different vegetation, fire and lightning emission scenarios, and to their (RO_2+HO_2) abundances. This information is used to calculate the relative importance of O_3 versus (RO_2+HO_2) in NO_x cycling, which determines the $\Delta^{17}O$ value of NO_2 and largely that of NO_3^-. We also use ICECAP to estimate the glacial–interglacial changes in the relative importance of each oxidation pathway from NO_2 to NO_3^-, thereby determining the overall changes in $\Delta^{17}O(NO_3^-)$ that originates from tropospheric chemistry. These are detailed in sections 5 and 6 of the Supplementary Information.

Data availability. The ice-core data that support the findings of this study are available from the NSF Arctic Data Center: https://arcticdata.io/catalog/#view/doi:10.18739/A23T0C.

32. Cuffey, K. M. & Clow, G. D. Temperature, accumulation, and ice sheet elevation in central Greenland through the last deglacial transition. *J. Geophys. Res.* **102,** 26383–26396 (1997).
33. Geng, L. *et al.* Analysis of oxygen-17 excess of nitrate and sulfate at sub-micromole levels using the pyrolysis method. *Rapid Commun. Mass Spectrom.* **27,** 2411–2419 (2013).
34. Geng, L. *et al.* On the origin of the occasional spring nitrate peak in Greenland snow. *Atmos. Chem. Phys.* **14,** 13361–13376 (2014).
35. Kaiser, J., Hastings, M. G., Houlton, B. Z., Rockmann, T. & Sigman, D. M. Triple oxygen isotope analysis of nitrate using the denitrifier method and thermal decomposition of N_2O. *Anal. Chem.* **79,** 599–607 (2007).
36. Gupta, P., Noone, D., Galewsky, J., Sweeney, C. & Vaughn, B. H. Demonstration of high-precision continuous measurements of water vapor isotopologues in laboratory and remote field deployments using wavelength-scanned cavity ring-down spectroscopy (WS-CRDS) technology. *Rapid Commun. Mass Spectrom.* **23,** 2534–2542 (2009).
37. Kaplan, J. O., Folberth, G. & Hauglustaine, D. A. Role of methane and biogenic volatile organic compound sources in late glacial and Holocene fluctuations of atmospheric methane concentrations. *Glob. Biogeochem. Cycles* **20,** GB2016 (2006).
38. Pfeiffer, M., Spessa, A. & Kaplan, J. O. A model for global biomass burning in preindustrial time: LPJ-LMfire (v1.0). *Geosci. Model Dev.* **6,** 643–685 (2013).
39. Alexander, M. J. *et al.* Recent developments in gravity-wave effects in climate models and the global distribution of gravity-wave momentum flux from observations and models. *Q. J. R. Meteorol. Soc.* **136,** 1103–1124 (2010).

© 2017 Macmillan Publishers Limited, part of Springer Nature. All rights reserved.